J Seismol (2009) 13:601–611
DOI 10.1007/s10950-009-9153-3

ORIGINAL ARTICLE

High frequency site amplification evaluated from Borehole data in the Taipei Basin

Ming-Wey Huang · Jeen-Hwa Wang · Hung-Hao Hsieh · Kuo-Liang Wen

Received: 10 September 2007 / Accepted: 15 January 2009 / Published online: 10 February 2009

Abstract Based on the quarter-wavelength approximation, the frequency-dependent site amplifications, $A(f)$, at 18 free-field strong-motion stations in and near the Taipei Basin are evaluated from well-logging data. The V_{30}, which is the average of the S-wave velocities in the topmost 30 m, is a significant factor in classifying the sites. Results show that the site amplifications at all sites in study are larger than 1 and functions of frequency. Compared with the Haskell method, the quarter-wavelength approximation is almost an average and a good representation of overall amplifications. It is noted that the site amplifications evaluated in this study can apply only to frequencies greater than about 1.1 Hz for class C sites and 3.1 Hz for class D.

M.-W. Huang (✉)
National Science and Technology Center
for Disaster Reduction, Sindian City 23143, Taiwan
e-mail: mwhuang@ncdr.nat.gov.tw

J.-H. Wang
Institute of Earth Sciences, Academia Sinica,
P.O. Box 1-55, Nangang, Taipei 115, Taiwan

H.-H. Hsieh · K.-L. Wen
National Center for Research
on Earthquake Engineering, Taipei 106, Taiwan

K.-L. Wen
Institute of Geophysics, National Central University,
Jung-Li, Taiwan

Keywords Site amplification · Quarter-wavelength approximation · Borehole data · Taipei Basin

1 Introduction

The site effect remarkably affects the ground motions. The seismic waves are amplified when they propagate through the low-shear velocity and low-density layers. The amplification of seismic waves is usually a function of frequency and stronger at a soil site than at a rock one. Numerous accelerographic stations are built on the soil sites, and thus, it is necessary to eliminate the site effects. Conventionally, four ways are applied to evaluate the site amplifications. The first way (Zhang 2004), which can only provide the relative amplification, is a comparison of the Fourier amplitude spectra at a site to that at a reference hard-rock site, with nearly flat response. However, it is actually not easy to locate a perfect reference site. The second way (Lermo and Chávez-García 1993) is the calculation of horizontal-to-vertical spectral ratio at a site. The first and second ways can only provide the relative site amplification. The third way (Atkinson and Cassidy 2000; Malagnini et al. 2004) is the division of the Fourier amplitude spectrum of recorded ground motions by that simulated based on a so-called absolute-source-spectra model, which is assumed to have no site

effects. For this way, the precise source spectra and path effects underneath a study site are needed. The fourth way (Haskell 1960; Joyner et al. 1981; Boore and Joyner 1997; Klimis et al. 1999; Huang et al. 2005, 2007) is a comparison between observed ground motions and values calculated on the basis of measured velocity model assuming 1-D wave propagation. However, it is not easy to apply this method because the comprehensive velocity and density models are usually not available. The third and fourth ways can give the absolute amplification.

From surficial geology, Lee et al. (2001) classified 708 free-field strong-motion station sites operated by the Central Weather Bureau in Taiwan into four categories, i.e., classes B, C, D, and E, using a scheme compatible with the 1997 Uniform Building Code provisions. Meanwhile, they also studied the response spectral shape in the period range 0–3 s and the horizontal-to-vertical spectra ratios in the period range 0.03–3 s. Results show frequency dependence of the site effect. However, their results can only be applied to engineering problems, yet not enough for scientific purposes. Zhang (2004) evaluated the site amplification with seismic-wave attenuation in the frequency range 0.7–6 Hz based on the site classification made by Lee et al. (2001). However, the site classification is needed to be re-classified as taking the well-logging data into account.

The Taipei Metropolitan Area (TMA), which is located on the Taipei Basin, is the political, economic, and cultural center of Taiwan. Although seismicity in the TMA is lower than elsewhere in Taiwan, numerous earthquakes still occur in and near the area (Hsu 1961, 1983a, b). Historical data show that a large earthquake occurred in the area in 1694, resulting in an earthquake-induced lake and destruction of numerous aboriginal houses. The magnitude of the event has been estimated by Hsu (1983b) to be 7. On April 15, 1909, an M7.3 earthquake took place at a depth of about 80 km beneath the area, with casualties including nine dead, 51 injuries, 122 houses that collapsed, and 1,054 houses damaged (Hsu 1961).

In the TMA, pre-1970 large distant earthquakes caused minor damages, while several post-1970 seismic events yielded remarkable damages (Wang 1998). Observations show that the predominant frequencies of seismic waves in the Taipei Basin generated by distant earthquakes are 0.5–1.0 Hz (Chen 2003). This would result in large damage to the buildings of ten to 20 floors. Before 1970, there were buildings with only few floors, usually less than four, and thus, the damage was small. Since 1970, a large number of high-rise buildings of ten to 20 floors or more have been constructed, and thus, the earthquake-induced damage increases, even with the quality of construction having been substantially upgraded. Meanwhile, the population has remarkably increased, a rapid transportation system has been in operation, and two nuclear power plants located in the vicinity of the area have been operated for a long time. Hence, much attention for seismic risk mitigation must be paid in the area.

Wen et al. (1995a, b) and Wen and Peng (1998) studied the characteristics of site effects on strong ground motions in the Taipei Basin. They numerically simulated 3-s ground motions by using the boundary integral method. However, the site effect for the 3-s seismic waves is not enough for the purpose of mitigating seismic risk. The TMA is situated on the Taipei Basin with thick recent deposits. The thick deposits would enhance the strong ground motions, thus leading to great damage, even though earthquakes occur far away from the area. From a comparison of *S*-wave velocity (V_s) model with the spatial distribution the PGA values averaged over 50 earthquakes, Wang et al. (2004) stated that larger PGA is associated with lower *S*-wave velocity. From the analyses of the strong ground motions generated from the March 31, 2002, Hualien, Taiwan earthquake, which was about 150 km far away from the basin, Chen (2003) observed that the seismic waves reflected from the Moho enlarged the ground motions at a small area in the eastern side of the basin.

From well-logging data of shear velocities and densities, an attempt is made to evaluate the absolute frequency-dependent site amplifications of shallow sediments at the 18 boreholes in the TMA using the method proposed by Boore and Joyner (1997). Also estimated are the averaged frequency-dependent site amplifications from the results of individual boreholes.

2 Geological setting

The Taipei Basin is specified with sedimentary layers (CGS 1999; Wang et al. 2004; Wang-Lee and Lin 1987). In the basin, Quaternary sediments lie on a Tertiary basement. The Quaternary sediments are composed of three formations, i.e., the Sungshan, Chingmei, and Hsinchuang formations from top to bottom. Teng et al. (1994) divided the Hsinchuang formation into two, i.e., the Wuku and Banchiao formations. Figure 1b shows the subsurface geological structures along Line AB depicted in the SE–NW direction as shown in Fig. 1a. The topmost part of the Sungshan formation is a soft layer, which is composed of unconsolidated sand, silt, and clay with a thickness varying from 50 m in the southeast to 120 m in northwest.

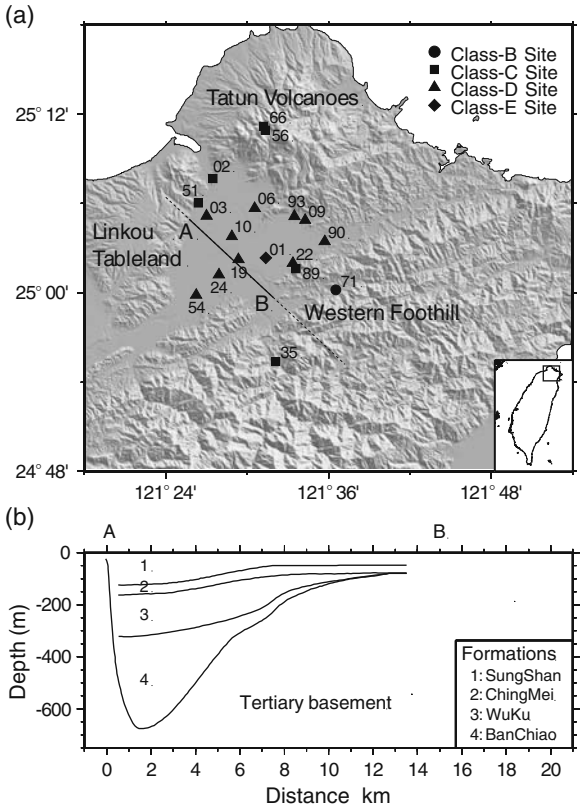

Fig. 1 **a** A map to show the Taipei Basin and surrounding geological provinces. The station sites in use are displayed in *circles*, *squares*, *triangles*, and *diamonds* for Class B, C, D, and E sites, respectively, and **b** subsurficial geological structures in the Taipei Basin (modified from Wang et al. 2004)

The lower part of the formation is dominated by silt. The Chingmei formation is full of gravels. The Hsinchuang formation is composed of sand and silt. From shallow reflection experiments and the borehole drilling results, Wang et al. (2004) found that the three layers of the Sungshan formation have low V_s, i.e., 170, 230, and 340 m/s, respectively. The values of V_s in the Chingmei, Wuku, and Banchiao formations are, respectively, 450, 600, and 880 m/s. The uncertainties of V_s are lower for the former formation than the latter two. The value of V_s of the Tertiary basement is ~1,500 m/s.

3 Method

Joyner et al. (1981) first introduced the quarter-wavelength approximation method to evaluate the frequency-dependent site amplifications. The amplification at a particular frequency is the squared root of the ratio of the seismic impedance (velocity × density) averaged over a depth range corresponding to a quarter wavelength to that at the depth of the source of seismic waves. Day (1996) made some theoretical justification on the method. The approximation is insensitive to the discontinuities in seismic velocities beneath a site and does not include nonlinear response due to the different input intensities of seismic waves and resonance due to subsurface topography.

In this approximation, incident-plane waves through attenuation corrections are taken into account. Boore and Joyner (1997) defined the amplification to be the ratio of the Fourier amplitude spectrum of unattenuated incident plane waves to that recorded at the surface of a uniform half-space by the same incident waves. The amplification decreases with wavelength and approaches unity for very long period waves. They denoted S_{tt}, $\beta_z = z/S_{tt}$, and ρ_z, respectively, to be the average S-wave travel time, the average velocity, and the average density. The average density is defined to be $S_{tt}^{-1} \cdot \Sigma(z_i \rho_i / \beta_i)$ where z_i, ρ_i, and β_i are, respectively, the thickness, density, and S-wave velocity in the ith layer in consideration. From the three quantities, the frequency, f, is $1/(4 \cdot S_{tt})$ and the site amplification, $A(f)$, is $(\rho_s \beta_s / \rho_z \beta_z)^{1/2}$, where the subscript "s" represents the source area, associated with the layer thickness of z from which

the seismic waves are incident to the sediments. The five quantities are all calculated from the ground surface to depth z.

4 Borehole data

As mentioned above, there are 11 boreholes inside the Taipei Basin. For the purpose of comparison, seven boreholes located outside but near the basin are also taken into account. The localities of the 18 boreholes are shown in Fig. 1a. The core samples of the 18 sites show that geological materials belong to the Sungshan formation, which is a soft layer and composed of unconsolidated sand, silt, and clay. The depths of the 18 boreholes range from 31 to 56 m. The majority of the boreholes have a depth of 30 m. The depths of two boreholes, respectively, at a class D site and a class E one are greater than 40 m.

In each borehole, V_s is measured at 0.5-m intervals. The depth profiles of V_s at four borehole sites, 71 (class B), 02 (class C), 09 (class D), and 01 (class E), are shown in Fig. 2b by a solid line. The total number of samples of V_s loggings is 1,126, and the measured values are in the range 93–1235 m/s. The ranges of measured shear velocities at the 18 boreholes are shown in Fig. 2b, where all sites are projected to line AB in Fig. 1. Except for few sites, the velocity range is smaller inside than outside the Taipei Basin. Inside the basin, except for sites 09 and 22, the maximum velocity is less than 500 m/s and is larger in the eastern side than in the western side of the basin. The US's criteria to classify sites (cf. Lee et al. 2001) are based on V_{30}, where V_{30} is the averaged shear-wave velocity in the topmost 30 m: $V_{30} > 1,500$ m/s for class A, $V_{30} = 760$–$1,500$ m/s for class B, $V_{30} = 360$–760 m/s for class C, $V_{30} = 180$–360 m/s for class D, and $V_{30} < 180$ m/s for class E. From well-logging data, it is necessary to re-classify 13 station sites, which have been classified by Lee et al. (2001) from surficial geology, in the Taipei Basin. Consequently, there is a class B site (denoted by

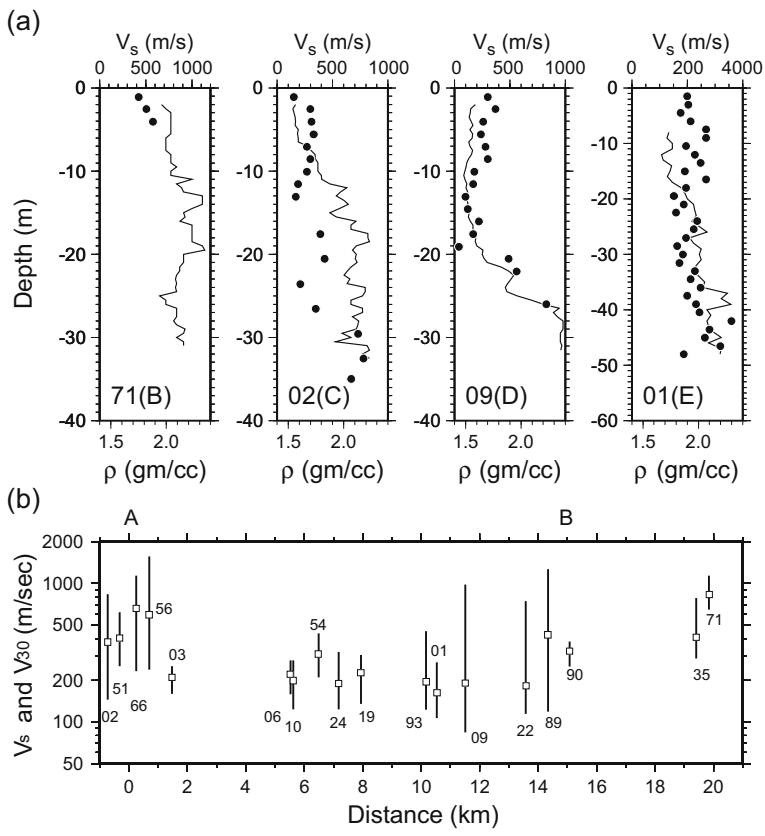

Fig. 2 **a** Four examples of well-loggings of *S*-wave velocity (*lines*) and density (*circles*) varied with depth and **b** the measured velocity range (in a *vertical line* segment) and V_{30} (in an *open square*) at each borehole site, whose station code is given in and locality is projected on line AB shown in Fig. 1a

a circle), six class C sites (denoted by squares), ten class D sites (shown by triangles), and a class E site (depicted by a diamond). Class B and C stations are located at the mountains outside the Taipei Basin, while class D and E stations inside the basin.

Unlike V_s, ρ was not measured regularly at 0.5-m intervals and was only done at 1 point in a specific geological layer. The total number of logging samples of ρ is 308, and the measured values are in the range 1.3–2.3 gm/cc. At some well-logging points, where only the V_s was measured, the value of ρ was assigned as that in the same geological formation at the same site or at a nearby one. A complete well-logging profile including the two parameters can thus be constructed at each borehole site. Included also in Fig. 2a are the values of ρ (denoted by a solid circle) at four borehole sites: 71 (class B), 02 (class C), 09 (class D), and 01 (class E).

An important site factor in predicting ground motions and in constructing the building codes (Boore and Joyner 1997) is the averaged shear velocity in the topmost 30 m that $V_{30} = 30/S_{tt}(30)$, which is plotted in Fig. 2b by an open square. Except for few sites, V_{30} is smaller inside than outside the basin. Unlike the maximum velocity, V_{30} is relatively uniform inside the basin. At sites 09 and 22, V_{30} is small, even though the maximum velocities are large. This means that lower V_s dominates the core samples at the two sites.

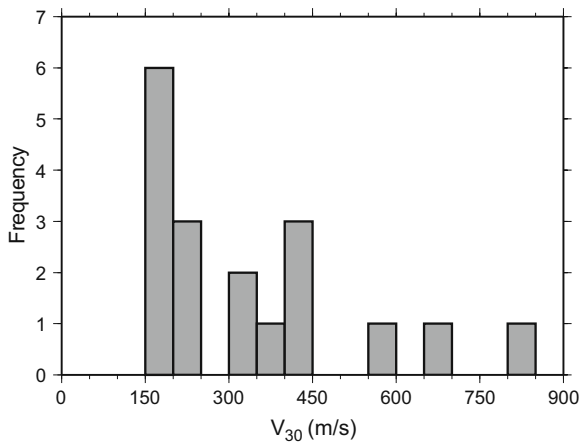

Fig. 3 Frequency of average shear-wave velocity in the topmost 30 m measured from well-logging data

Figure 3 displays the frequency distribution of V_{30}. Obviously, the V_{30} distributes in a wide velocity range and the frequency decreases with increasing velocity.

Figure 4a shows that the S_{tt} increases with depth z. There are four peculiar variations of S_{tt} versus depth in Fig. 4b. Two of them are related to class C sites (02 and 89), which are located at the mountains, respectively, to the west and east of the basin. The values of S_{tt} with depths less than 8 m at the two sites are larger than or equal to those at other class C sites and two class D ones (54 and 90; see Fig. 4b). This indicates that at the two class C sites, V_s is abnormally low for $z < 8$ m.

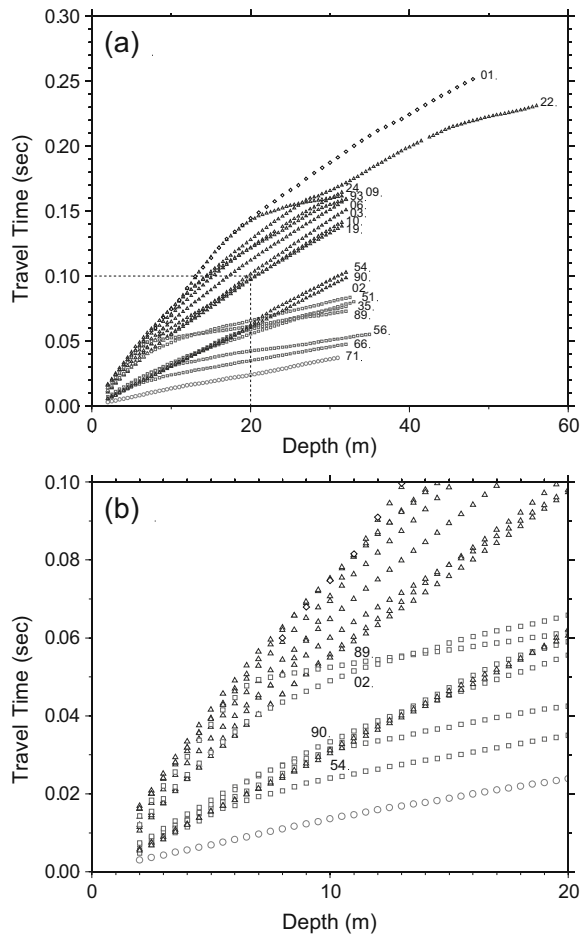

Fig. 4 **a** *S*-wave travel time versus depth: *circles*, *squares*, *triangles*, and *diamonds* for class B, C, D, and E sites, respectively. **b** Enlarged figure of *dashed region* in **a**, symbols are same as in **a**

In addition, S_{tt} first increases with depth in a larger slope for $z < 8$ m and then in a smaller one for $z > 8$ m. This leads to the same change for the shear velocity. This yields larger V_{30} at the two sites, and thus, they are re-classified into class C. Of course, they could also be classified into class D when only the value of V_s for $z < 8$ m is taken into account. Although the values of S_{tt} at two class D sites (54 and 90) are distributed within the class C group, they can be classified into class D because V_{30} are, respectively, 310 and 325 m/s at the two sites. It is noted that the two values of V_{30} are almost near the lower bound of class D. It can be seen from Fig. 4b that at the two class D sites, the increasing rate of S_{tt} with depth is constant in the whole borehole depth, while at the class C sites, the rate decreases almost at 10-m depth for some boreholes and at 18-m depth for others. This means that at class C sites, V_s increases at the two depths, thus leading to larger V_{30}. Of course, the two class D sites could be classified into class C when only the values of V_s in $z < 10$ m or in $z < 18$ m are given. Results suggest that V_{30} is the optimum factor in classifying the station site.

5 Amplifications from Borehole data

There are two steps for calculating the frequency-dependent site amplifications of shallow sediments relative to the Tertiary basement in the Taipei Basin. On the first step, the amplifications as a function of frequency at each site are evaluated. For this evaluation, the values of β_s and ρ_s of the basement are needed. Fletcher and Wen (2005) took 1,200 m/s from Wen and Peng (1998) to be the V_s of the Tertiary basement. This value was inferred by Wang et al. (1996) from seismic reflection surveys conducted before 1996. From more shallow seismic reflection data incorporated with borehole data, Wang et al. (2004) revised their 1996 V_s model of the basin. The updated model can be seen in the website: http://tao.cgu.org.tw/pdf/v154p609.pdf. From the new velocity model, we take the average shear velocity, i.e., 1500 m/s, of the Tertiary basement to be β_s. There is no any detailed density model right below the basin due to limited gravity data. From the gravity survey in the Tatun Volcano Group (TVG), just north of the basin, Tzou and Yu (1987) inferred that, from top to bottom, there are three layers with different densities: 2.40 gm/cc in the range 0–400 m, 2.45 gm/cc in the range 400–1,600 m, and 2.55 gm/cc below 1600 m. Inside the basin, the thicknesses of sediments are 100–700 m; while outside the basin, the sediments become thin. The 3-D velocity tomography (Ma et al. 1996) shows that the deeper structures below the TVG are similar to those under the basin. Hence, we can take the density (=2.45 gm/cc) of the second layer of the TVG to be ρ_s under the

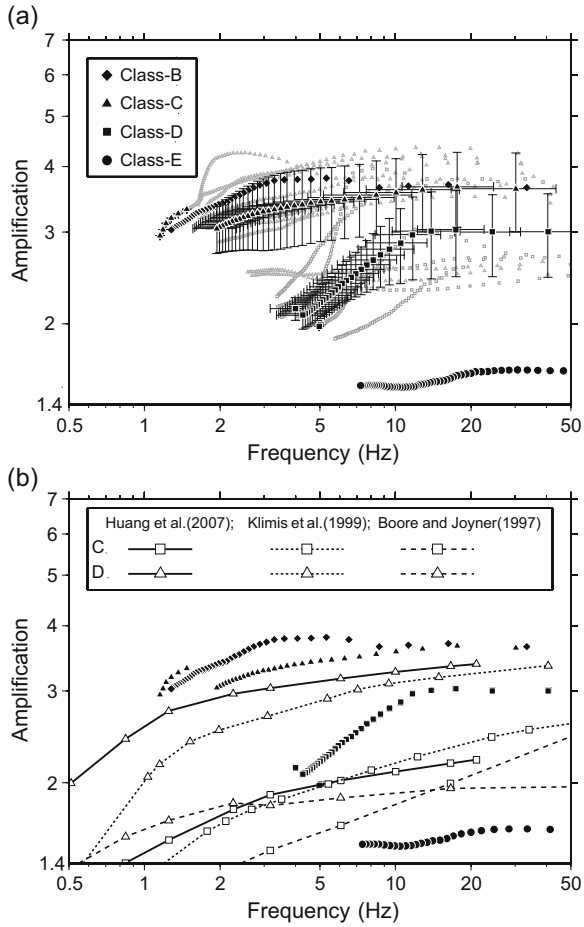

Fig. 5 The plots of $A(f)$ versus f: *circles*, *squares*, *triangles*, and *diamonds* for class B, C, D, and E sites, respectively. **a** The average values, with error bars, from various boreholes at the same depth are displayed by *solid symbols*. **b** Site amplification functions in this study are compared with those of Huang et al. (2007), Klimis et al. (1999), and Boore and Joyner (1997)

basin. From the well-logged values of V_s and ρ, we calculate $A(f)$ and f at a single site. The plots of $A(f)$ versus f are displayed in Fig. 5 with different symbols: solid circles, open squares, open triangles, and solid diamonds, respectively, for the class B, C, D, and E sites. The frequency ranges are different for the four classes of sites. The parameter $V_{30} = 30/S_{tt}(30)$ (in m/s) controls the magnitude of lower-bound frequency, f_{low}, associated with the topmost 30 m. The calculated values of V_{30} are 832.5 and 162.0 m/s, respectively, for class B and E sites, and in the range of 375.7–661.1 m/s for class C and 182.4–324.6 m/s for class D. Therefore, the values of f_{30} are 6.9 Hz for class B site, 3.1–5.5 Hz for class C, 1.5–2.7 Hz for class D, and 1.3 Hz for class E. As taking the deepest borehole of each class into account, f_{low} is 6.9 Hz for class B site, 3.1 Hz for class C, and 1.1 Hz for class D and E. This can be seen from Fig. 5 that, except for few boreholes deeper than 30 m, there are no data points for $f < 3$ Hz for class C sites. According to V_{30}, the plots can be divided into four groups, which are associated, respectively, with class B, C, D, and E sites from bottom to top. Of course, the plots of the unique class E site are inside the class D group.

On the second step, the average amplifications are calculated from those of individual sites at the same borehole depth. For a particular depth, the frequencies at different sites vary in a small range due to unequal velocity profiles. The average frequency is just the frequency related to such depth. The values of $A(f)$ at several frequencies are shown in Table 1. Since there is only one site for classes B and E, it is not necessary to take the average for them. When $f < 2.3$ Hz, the numbers of well-logged data for class D sites are also only one (see Table 1). The data points of average amplification versus average frequency are displayed in Fig. 5 by the solid symbols, i.e., circles, squares, triangles, and diamonds, respectively, for classes B, C, D, and E. Included also in Fig. 5 are the error bars of $A(f)$ and f for classes C and D. At the class B site, $A(f)$ first slightly decreases and then increases with increasing f from 7 to 50 Hz. $A(f)$ varies in a small range 1.5–1.6. At class C sites, average $A(f)$ first increases with f and then becomes a constant of ~3.0 when average $f > 12$ Hz. However, the value of $A(f)$ at $f = 3.5$ Hz is larger than that at $f = 4$ Hz. At class D sites, average $A(f)$ first increases with f and suddenly drops to a small value at $f = 2$ Hz, then increases with f again, and finally becomes a constant of ~3.6 when $f > 10$ Hz. When $f < 10$ Hz, the increasing rate is much larger for class C sites than for class D ones. When $f > 10$ Hz, the data points for classes C and D are somewhat below the individual trend. This might be due to lower reliability of measured values at shallow depths because it is not easy to exactly measure the values of V_s and ρ in the fragmented soil layers from seismic reflections. At the class E site, $A(f)$ first increases and then decreases with increasing f. $A(f)$ varies from 3.0 to 3.8, with a peak at $f = 2$ Hz. The amplifications at the class E site approach 3.6 when $f > 7$ Hz.

Table 1 The values of $A(f)$ at several frequencies for four classes of sites

f (Hz)	Class B	Class C	Class D	Class E
1.1			2.8 (1)	3.0 (1)
1.3			3.2 (1)	3.0 (1)
1.5			3.3 (1)	3.2 (1)
2.0			3.1 (1)	3.4 (1)
2.3			3.2 (10)	3.5 (1)
2.7			3.2 (10)	3.6 (1)
3.1		2.0 (1)	3.3 (10)	3.7 (1)
4.0		2.1 (3)	3.4 (10)	3.8 (1)
5.0		2.2 (6)	3.4 (10)	3.8 (1)
6.0		2.4 (6)	3.5 (10)	3.8 (1)
6.9	1.5 (1)	2.6 (6)	3.5 (10)	3.7 (1)
11.0	1.5 (1)	2.9 (6)	3.6 (10)	3.7 (1)
25.0	1.6 (1)	3.0 (6)	3.6 (10)	3.6 (1)
30.0	1.6 (1)	3.0 (6)	3.6 (10)	3.6 (1)

The number of boreholes at the same depth used in estimating the values $A(f)$ is given in the parentheses

6 Discussion

As shown in Fig. 5, $A(f)$ at the unique class B site, which is located at the base rock of the Miocene formation, first decreases and then increases with increasing f. In the frequency range 7–50 Hz, the amplifications are very stable and vary only in a small range 1.5–1.6. This site was commonly selected to be a reference one for evaluating the relative site amplifications at the soil sites in the basin. The present results show that in this frequency range, the relative site amplifications calculated based on this reference site would be underestimated and 1.5–1.6 times smaller than those evaluated from a perfect hard rock model. Since there is only one amplification–frequency function at the class B site, it cannot be regarded as a representative of such a class of sites. At the unique class E site, $A(f)$ first increases and then decreases with increasing f, with a peak almost at $f = 3$ Hz. The amplifications at this site are smaller than those at all class D sites when $f < 1.7$ Hz but opposite when $f > 1.7$ Hz. Nevertheless, the V_{30} at this site is less than those of several class D sites because the values of V_s in the topmost 10 m are smaller at this site than the latter ones. It can also be seen from Fig. 4 that S_{tt} at this site is less than those at several class D sites when $z < 12$ m, yet opposite when $z > 12$ m. This class E site is located at a particular area with large site amplifications in the basin (Wen and Peng 1998; Chen 2003). Since only one amplification–frequency function at the unique class E site is available, a solid conclusion cannot be exactly reached for this particular area. The amplification–frequency functions first increase with f and then become flat when $f > 12$ Hz and $f > 10$ Hz, respectively, at class C sites and at class D ones. This implicates a uniform velocity structure in very shallow depths underneath the two kinds of sites because the density is almost constant.

As shown Fig. 5b, the averaged amplification functions in Taipei Basin are compared with those of Huang et al. (2007) in central Taiwan (denoted by solid lines), Klimis et al. (1999) in Greece (denoted by dotted lines), and Boore and Joyner (1997) in North America (denoted by dashed lines). The lines with open squares represent the amplification functions of class C sites, while the lines with open triangles display those of class D sites. Before comparing the amplification functions, we modify the amplifications of the three regions because the settings of ρ (=2.8 gm/cc) and β (=3,500 m/s) at a basement depth of ~8 km are different from this study ($\rho_s = 2.45$ gm/cc and $\beta_s = 1500$ m/s of Tertiary basement with the deepest depth of ~0.7 km). The site amplifications are evaluated from $A(f) = (\rho_s\beta_s/\rho_z\beta_z)^{1/2}$ and a constant due to the difference of source parameters is $(\rho_s\beta_s/\rho\beta)^{1/2} = 0.61$. The site amplification functions of Huang et al. (2007), Klimis et al. (1999), Boore and Joyner (1997) are modified by a value of 0.6 and shown in Fig. 5b. Obviously, the amplification functions of classes C and D in North America depart from those in Taipei Basin. For class C sites, the difference in amplification functions between the Taipei Basin and central Taiwan and that between the Taipei Basin and Greece increase with frequency. For class D sites, the difference of amplification functions between the Taipei Basin and Greece decreases with frequency, while the difference between the Taipei Basin and central Taiwan increase slightly with frequency.

Since V_s and ρ are higher at the unique class B site than at others, the amplifications are larger at this site than at others. When $f < 10$ Hz, the difference in amplifications between any two classes of sites is dependent upon frequency. When $f > 10$ Hz, the amplifications at class C and D sites are, respectively, 1.9 and 2.3 times larger than those at the unique class B site, and those at class D sites are about 1.2 times larger than those at class C ones. The amplifications at the unique class E site are approximately equal to those at class D sites. This means that the velocity and density models at very shallow depths below the two classes of sites are similar.

In order to examine the quarter-wavelength approximation proposed by Boore and Joyner (1997), the theoretical amplification functions of seismic waves propagating through the shallow velocity models obtained from well-loggings are calculated using the propagator-matrix method of Haskell (1960). The computed amplifications in terms of frequency at different sites are shown by the gray lines in Fig. 6. Depicted also in Fig. 6

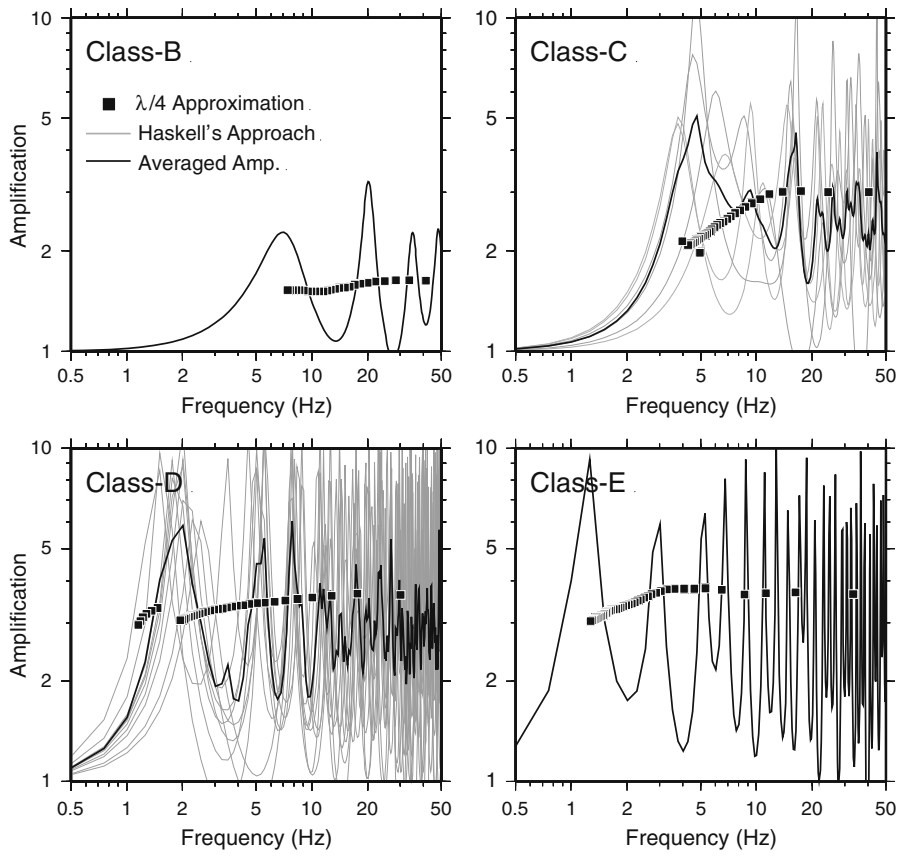

Fig. 6 The plots of $A(f)$ versus f: results calculated from the quarter-wavelength approximation (*squares*) and those from the Haskell's approach (*gray and black lines*) for class B, C, D, and E sites

are the average amplification–frequency functions by a solid line. There are numerous modes of resonant response of subsurface structures. The number of modes increases from class B to class E. In other words, the number of modes increases with decreasing V_s. The frequency of the average fundamental mode varies for different classes: 7 Hz for class B, 5 Hz for class C, 2 Hz for class D, and 1.5 Hz for class E. Fletcher and Wen (2005) observed that the fundamental mode of resonant response of the basin is at frequencies of at least 0.5 Hz. Their values are smaller than those of this study because their values are the response of the basin that has a depth much greater than the borehole depth of 30 m of this study. A wider frequency band can be computed either from deeper well-logged velocities or from a velocity model combining the well-logged velocities and those at depths evaluated from reflection seismology.

Included in Fig. 6 (displayed by solid squares) are the site amplifications evaluated from the quarter-wavelength approximation (Boore and Joyner 1997). From Boore and Joyner (1997), the quarter-wavelength approximation is almost an average and a good representation of overall amplifications. In addition, there are some advantages: low sensitivity to the layering in the system, a short computational time, and back-of-the-envelope estimates of site amplifications. Well-loggings can only be applied to evaluate the high-frequency site amplifications. In order to estimate seismic hazards in the TMA, it needs a comprehensive amplification–frequency function including the values at low frequencies for all classes of sites. The study is ongoing, and the results will be presented in the near future.

Although the frequency range of $f > 10$ Hz is not the engineering interest, it is still significant in studying grain-size-dependent dynamic behavior of soils. For a practical purpose, the natural frequency for regular civil structures is in the range 0.1–10 Hz. In this study, the lower bound

frequency is higher than 1.1 Hz. It is noted that the site amplifications can apply only to frequencies greater than about 1.5 Hz. Therefore, the amplifications at lower frequencies in the study area will be evaluated using a velocity model constructed from the 3D tomography inferred from *P*- and *S*-wave travel times. This study will be completed in near future.

7 Conclusions

From the quarter-wavelength approximation method by Boore and Joyner (1997), we evaluate the frequency-dependent site amplifications at 18 free-field strong-motion stations in the Taipei Metropolitan Area from well-logging data. V_{30} is a significant factor in classifying the sites. Results show that the site amplifications at all sites in study are larger than 1 and a function of frequency. At the class B site, $A(f)$ first slightly decreases and then increases with increasing f, varying from 1.5 to 1.6. At class C sites, average $A(f)$ first increases with f and then almost becomes a constant of ~3.0 when average $f > 12$ Hz. At class D sites, average $A(f)$ first increases with f and suddenly drops to a small value at $f = 2$ Hz, then increases with f again, and finally almost becomes a constant of ~3.6 when $f > 10$ Hz. At the class E site, $A(f)$ first increases and then decreases with increasing f, varying from 3.0 to 3.8, with a peak at $f = 2$ Hz. Compared with the Haskell method, the quarter-wavelength approximation is almost an average and a good representation of the overall amplifications. Since there is only one site, the amplification function cannot represent the averaged site response of classes B and E. However, the site amplifications evaluated in this study can be applied only to frequencies greater than ~1.1 Hz for class C and 3.1 Hz for class D.

Acknowledgements The authors would like to express their thanks to the Editor and two reviewers for useful comments. This study was financially supported by Academia Sinica under Grant No. AS-94-TP-A08 and the National Sciences Council under Grant No. NSC96-2116-M-001-012-NY3.

References

Atkinson GM, Cassidy JF (2000) Integrated use of seismograph and strong- motion data to determine soil amplification: response of the Fraser River Delta to the Duvall and Georgia Strait earthquake. Bull Seismol Soc Am 90:1028–1040. doi:10.1785/0119990098

Boore DM, Joyner WB (1997) Site amplifications for generic rock sites. Bull Seismol Soc Am 87:327–341

CGS (Central Geological Survey) (1999) Subsurface geology and engineering environment of the Taipei Basin. Special Pub. 11, Central Geol. Survey, Ministry of Economic Affairs, ROC, 406 pp (in Chinese)

Chen KC (2003) Strong ground motion and damage in the Taipei Basin from the Moho reflected seismic waves during the March 31, 2002, Hualien, Taiwan, earthquake. Geophys Res Lett 30(11):1551. doi:10.1029/2003GL017193

Day SM (1996) RMS response of a one-dimensional half space to SH. Bull Seismol Soc Am 86:363–370

Fletcher JB, Wen KL (2005) Strong ground motion in the Taipei basin from the 1999 Chi-Chi, Taiwan, Earthquake. Bull Seismol Soc Am 95:1428–1446. doi:10.1785/0120040022

Haskell NA (1960) Crustal reflection of plane SH waves. J Geophys Res 65:4147–4150. doi:10.1029/JZ065i012p04147

Hsu MT (1961) Seismicity of Taiwan (Formosa). Bull Earthq Res Inst Univ Tokyo 39:831–847

Hsu H (1983a) Source materials on the history of natural disasters in Ching Taiwan. Hazards Mitig Sci Technol Rep 72–01:5–6

Hsu H (1983b) Estimation of earthquake magnitudes and seismic intensities of destructive earthquakes in the Ming and Ching Eras. Meteorol Bull 29(4):1–18 (in Chinese)

Huang MW, Wang JH, Hsieh HH, Wen KL, Ma KF (2005) Frequency-dependent sites amplifications evaluated from well-logging data in central Taiwan. Geophys Res Lett 32:L21302. doi:10.1029/2005GL023527

Huang MW, Wang JH, Ma KF, Wang CY, Hung JH, Wen KL (2007) Frequency-dependent site amplifications with f ≥ 0.01 Hz evaluated from velocity and density models in central Taiwan. Bull Seismol Soc Am 97(2):624–637. doi:10.1785/0120060139

Joyner WB, Warrick RE, Fumal TE (1981) The effect of Quaternary alluvium on strong ground motion in the Coyote Lake, California, earthquake of 1979. Bull Seismol Soc Am 71:1333–1349

Klimis NS, Margaris BN, Koliopoulos PK (1999) Site-dependent amplification functions and response spectra in Greece. J Earthqu Eng 3(2):237–270. doi:10.1142/S1363246999000107

Lee CT, Cheng CT, Liao CW, Tsai YB (2001) Site classification of Taiwan free-field strong-motion stations. Bull Seismol Soc Am 91:1283–1297. doi:10.1785/0120000736

Lermo J, Chávez-García FJ (1993) Site effect evaluation using spectral ratios with only one station. Bull Seismol Soc Am 83:1574–1594

Ma KF, Wang JH, Zhao D (1996) Three-dimensional seismic velocity structure of the crust and uppmost mantle beneath Taiwan. J Phys Earth 44:85–105

Malagnini LK, Mayeda LK, Akinci A, Bragato PL (2004) Estimating absolute site effects. Bull Seismol Soc Am 94:576–590. doi:10.1785/012003161

Teng LS, Wang SC, Chang CB, Hsu C, Yuan PB, Chen PY (1994). Quaternary strata frame of the Taipei basin. Proc. joint symposium on Taiwan quaternary (5) and on investigation of subsurface geology/engineering environment of Taipei Basin, pp 129–135 (in Chinese)

Tzou YH, Yu GK (1987) Subsurface structure of the Tatun volcano group area inferred from the gravity data. Bull Geophys Natl Cent Univ 27/28:45–60

Wang JH (1998) Studies of earthquake seismology in Taiwan during the 1897–1996 period. J Geol Soc China 41:291–336

Wang CY, Lee YH, Chang HC (1996) P- and S-wave velocity structures of the Taipei basin. In: Symposium on Taiwan strong motion instrumentation program (II). Central Weather Bureau, pp 171–177

Wang CY, Lee YH, Ger ML, Chen YL (2004) Investigating subsurface structures and P- and S-wave velocities in the Taipei Basin. Terr Atmos Ocean Sci 14:609–628

Wang-Lee CM, Lin TP (1987) The geology and land subsidence of the Taipei Basin. Mem Geol Soc China 9:447–464

Wen KL, Peng HY (1998) Site effect analysis in the Taipei Basin: results from TSMIP network data. Terr Atmos Ocean Sci 9(4):691–704

Wen KL, Fei LY, Peng HY, Liu CC (1995a) Site effect analysis from the records of the Wuku downhole array. Terr Atmos Ocean Sci 6(2):285–298

Wen KL, Peng HY, Liu LF, Shin TC (1995b) Basin effects analysis from a dense strong motion observation network. Earth Eng Struct Dynam 24(8):1069–1083. doi:10.1002/eqe.4290240803

Zhang F (2004) Site response and attenuation analysis using strong motion and short-period data. Ph.D. Dissertation, Dept Civil Struct Environ Eng, SUNY-Buffalo, 278 pp